Supplementary Information for

An integrated microfluidic device for multiplexed imaging on spatial gene expression patterns of *Drosophila* embryos

Hongcun Zhu[1], Wenting Shen[2], Chunxiong Luo[1,2,3,*], Feng Liu[2,4,*]

[1] *The State Key Laboratory for Artificial Microstructures and Mesoscopic Physics, School of Physics, Peking University, Beijing, 100871, China*

[2] *Center for Quantitative Biology, Peking University, Beijing, 100871, China*

[3] *Wenzhou Institute University of Chinese Academy of Sciences, Wenzhou, Zhejiang, China;*

[4] *Key Laboratory of Hebei Province for Molecular Biophysics, Institute of Biophysics, School of Health Science & Biomedical Engineering, Hebei University of Technology, Tianjin, 300130, China*

Email: Feng Liu, liufeng-phy@pku.edu.cn; Chunxiong Luo, pkuluocx@pku.edu.cn

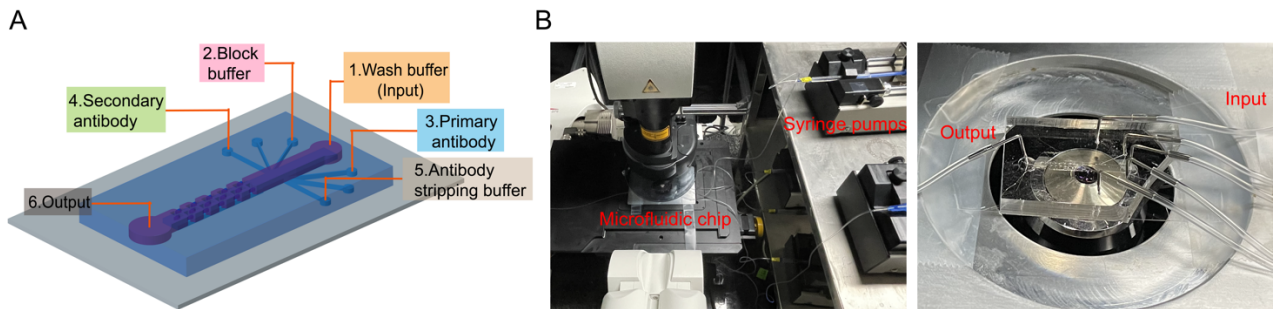

Fig. S1 Schematic and images of the integrated microfluidic systems. (A) An example of the diagram of the pipe connection. (B) The image of the microfluidic systems (left) and the chip connected the multiple regent tubes (right) during the microscope imaging.

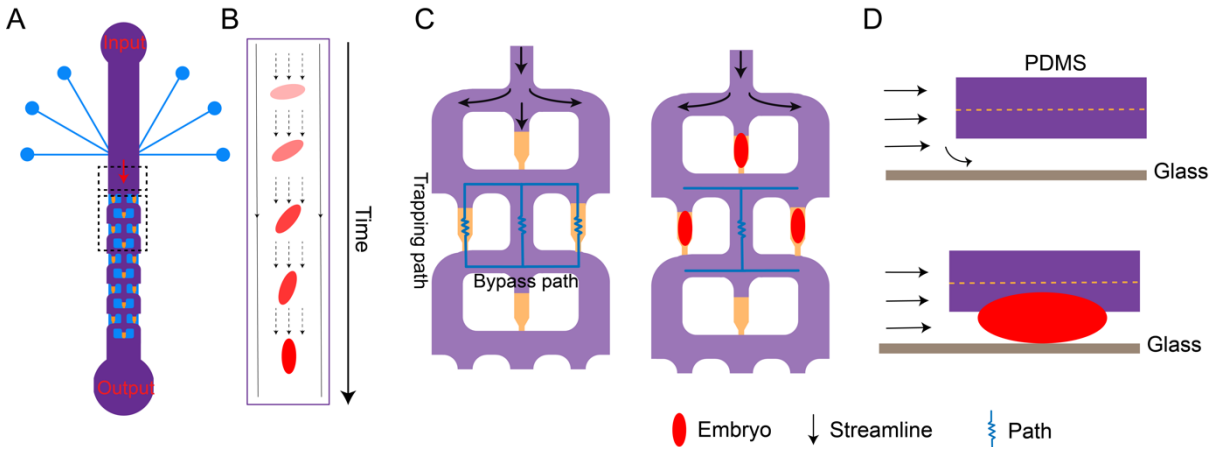

Fig. S2 Embryo capture process on chip. (A) Top view of the chip. (B) The process of the embryo rotating and aligning its major axis to be parallel to the flow direction in the loading channel before the trapping module (enlarged upper dotted box in (A)). (C) The streamline and flow resistance distribution on the trap path and the bypass path in the trapping module (enlarged down dotted box in (A)) before (left) and after (right) embryos are trapped. (D) The lateral view of the trapping unit before (up) and after (down) the embryo is trapped.

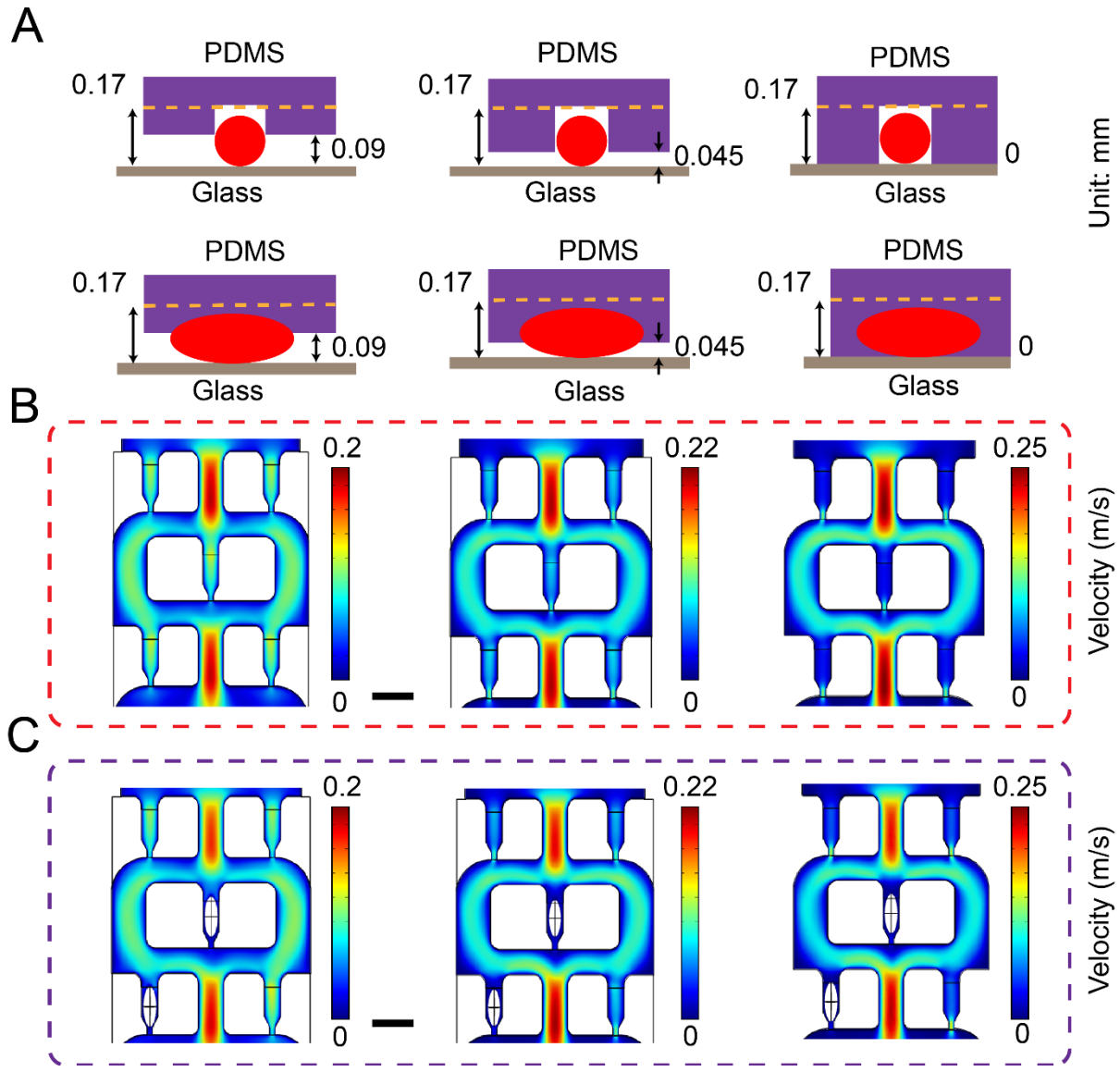

Fig. S3 Comparison of the simulated flow velocity of the trapping module with varying base layer heights. (A) The front (up) and side (down) view of the trapped embryos (red) and the trap unit with the base layers of different heights. (B-C) The simulated velocity distribution of the flow at the plane of 95 μm from the glass side when the flow velocity was set as 0.03 m/s by COMSOL (B) before and (C) after embryos are captured in some trapping units. The height of the base layer varies from 0.09 mm (left), 0.045 mm (middle), to 0 mm (right) as shown in (A). Scale bar, 500 μm.

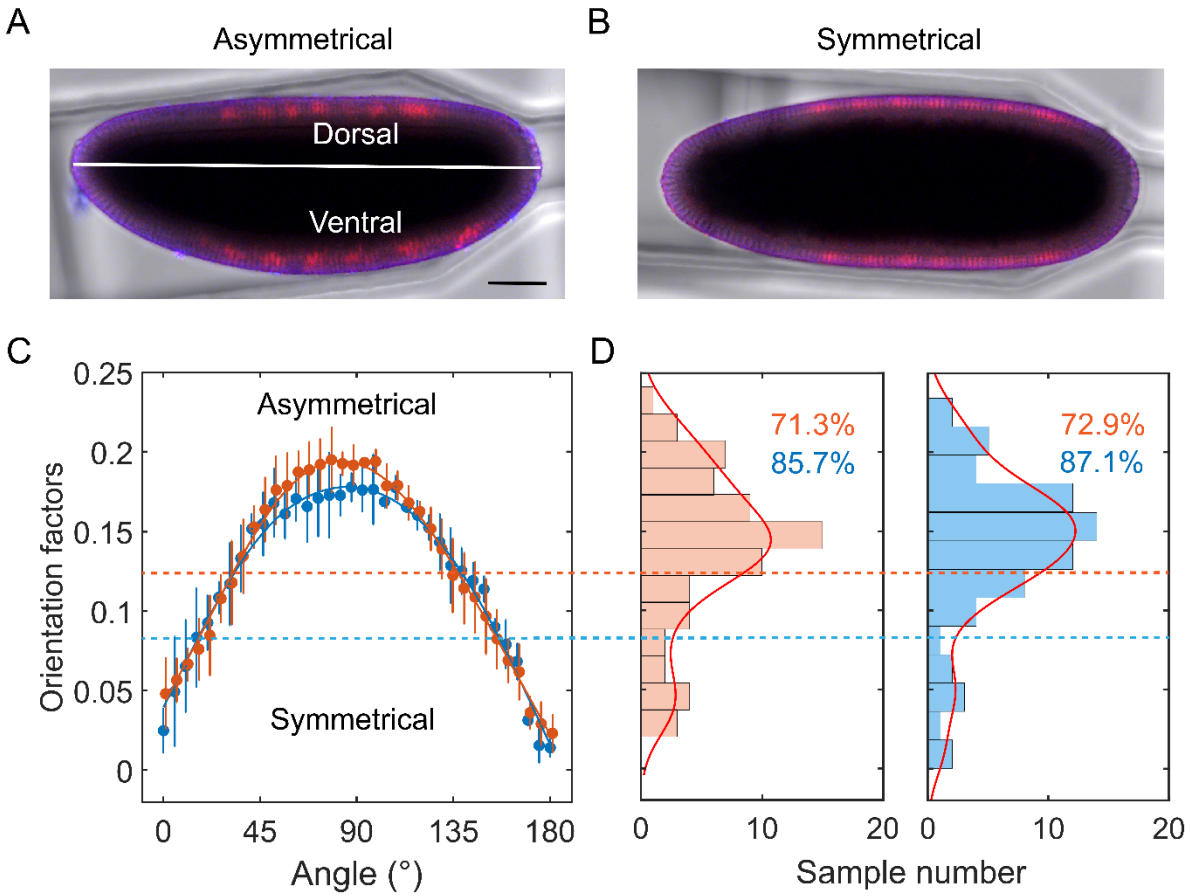

Fig. S4 Characterization of the orientation selectivity of the *Drosophila* embryos trapped with the microfluidic device. (A-B) Raw images of typical (A) asymmetrical orientation corresponding to the lateral view and (B) symmetrical orientation corresponding to the dorsal or ventral view of embryos. Scale bar, 50 μm. (C) The orientation factors (Factor 1, red; Factor 2, blue, see Materials and methods) as a function of the rotation angles around the AP axis with a 3D embryo from our previous research.[1] The blue (0.08 for Factor 1, and 0.075 for Factor 2, corresponding to the valley between the two peaks in (D)) and red (0.123 for Factor 1, and 0.121 for Factor 2, represent the average value corresponding to the rotation angle of 45° and 135°) dotted line represents the threshold value for the separation between the symmetry and asymmetry orientation. The error bars represent the standard deviation (sample size $N > 5$). (D) The histogram of the embryo distributions calculated with the two orientation factors (left, right) counted with all samples trapped by the microfluidic chip ($N = 70$). The *y* axis was the same as in (C). The asymmetry orientation (above the blue dotted line) accounts for 85.7 % (Left, red) and 87.1 % (Right, blue) of the trapped embryos according to Factor 1 and 2, respectively. And the asymmetry percentage above the red dotted line is 71.3 % for Factor 1 (Left, red) and 72.9 % for Factor 2 (Right, blue).

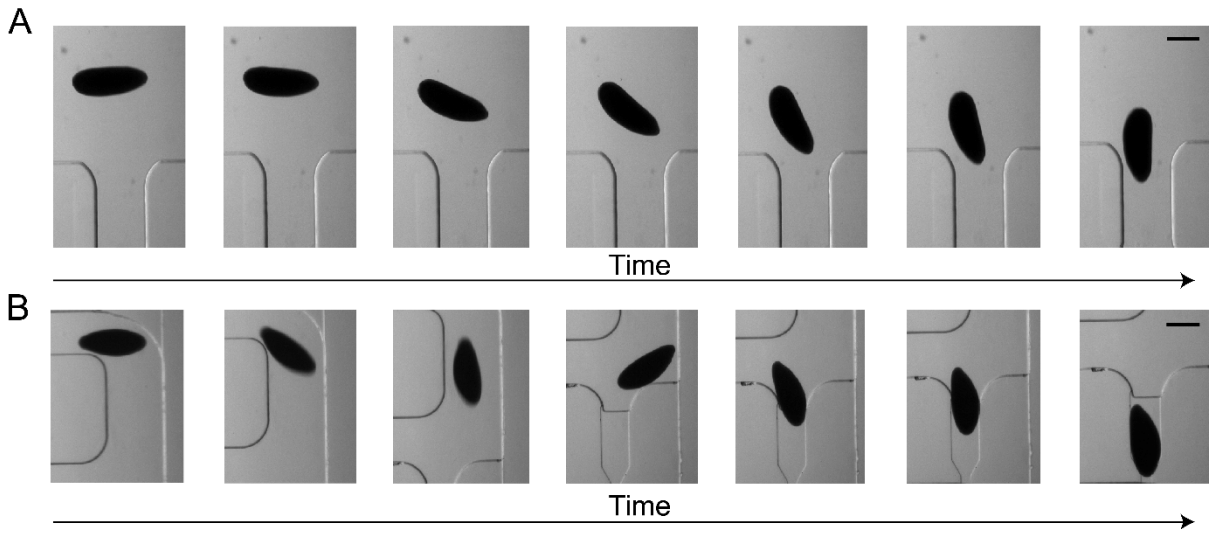

Fig. S5 Embryo orientation rearrangement in the hydrodynamic flow on-chip. (A) The snapshots of the rotating embryo aligning its major axis to be parallel to the flow direction before entering the trapping module. (B) The snapshots of the rotating embryo being guided into the trap unit by the hydrodynamic flow. Scale bar, 200 μm.

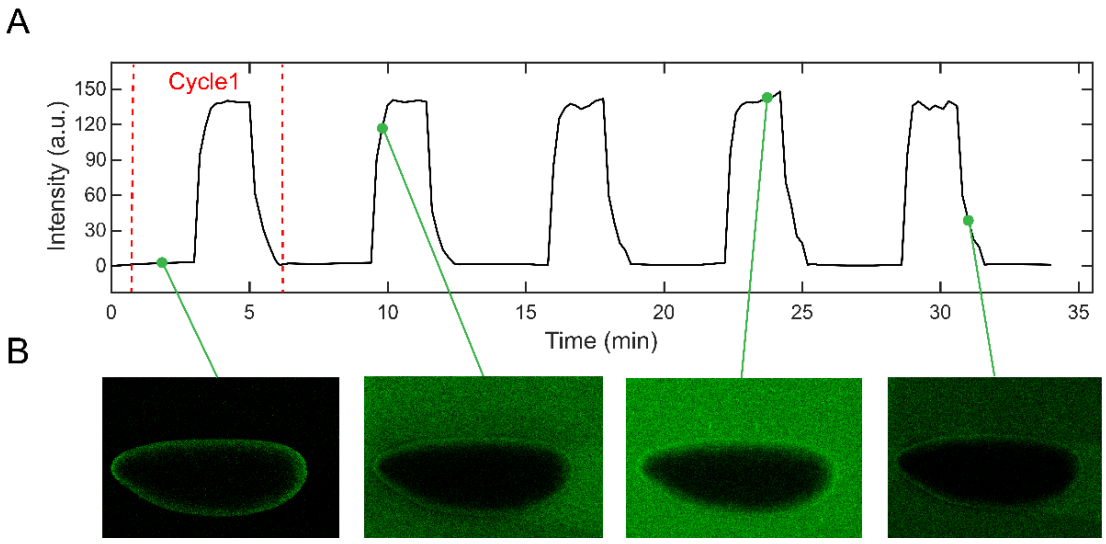

Fig. S6 Characterization of reagent delivery with multiple cycles. (A) The fluorescence intensity of secondary antibody reagent in the microfluidic channel as a function of processing time. (B) The snapshots at different time points in the cycle shown in (A).

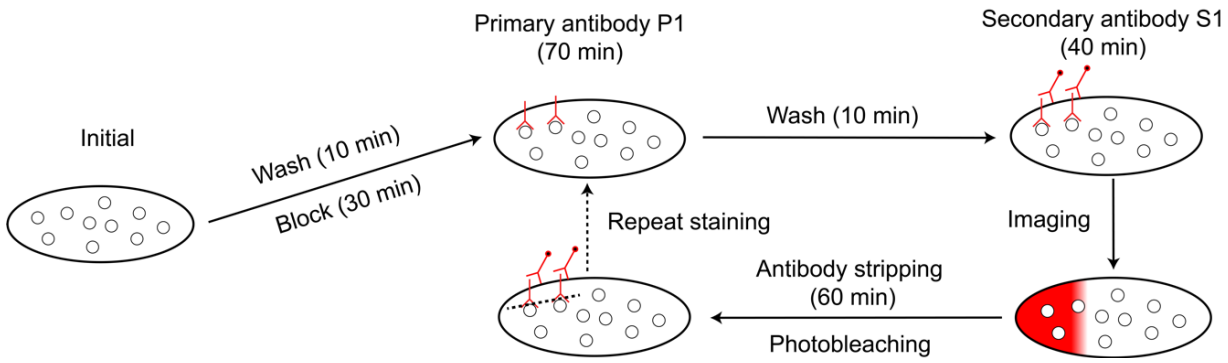

Fig. S7 Schematic of the general protocol for the indirect IF staining on-chip.

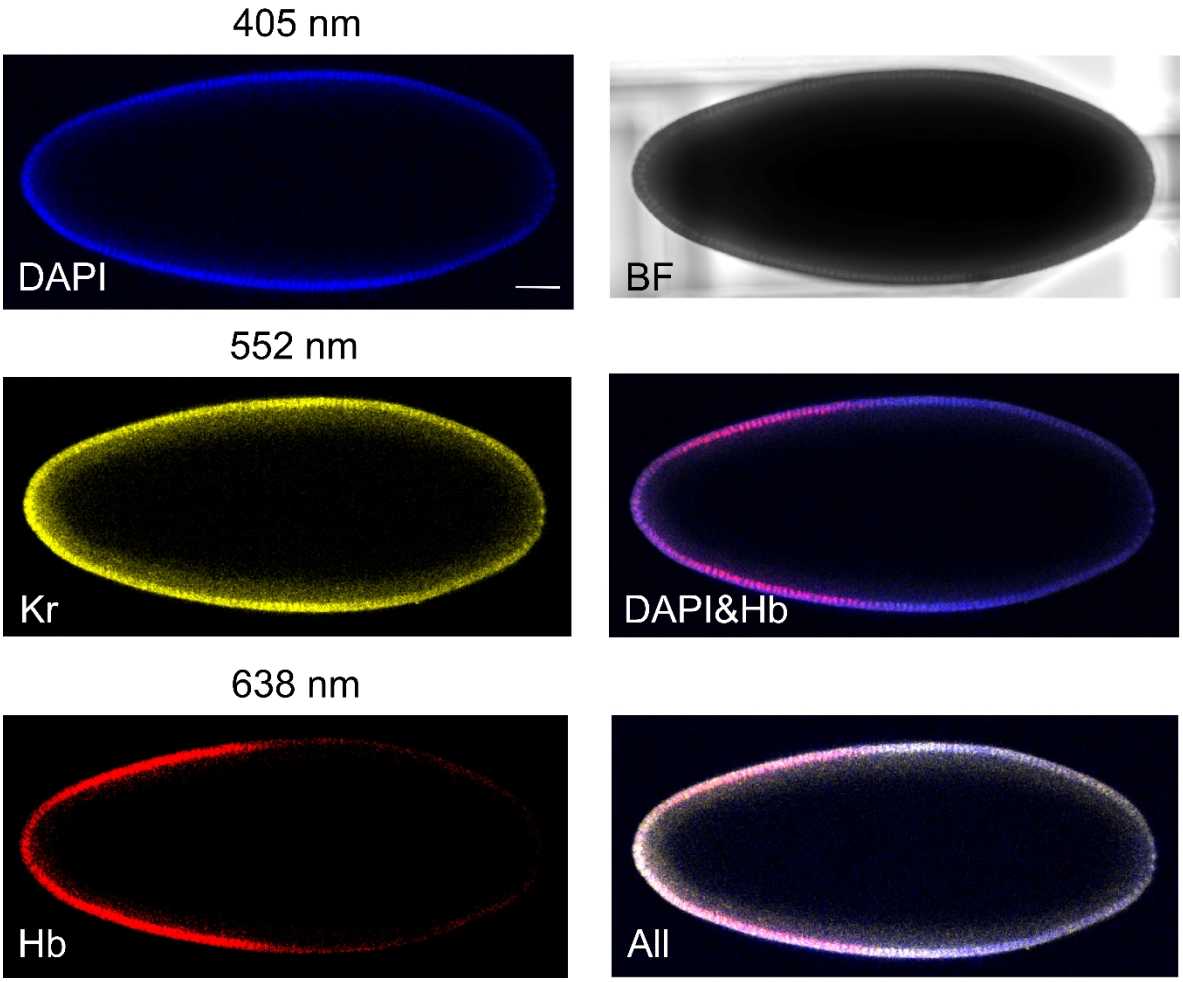

Fig. S8 Raw confocal images (left) of DAPI (blue), Kr (yellow) and Hb (red) of a representative fixed embryo of WT with the excitation wavelength of 405 nm, 552 nm, and 638 nm. The BF and merged images are shown on the right side. Scale bar, 50 μm.

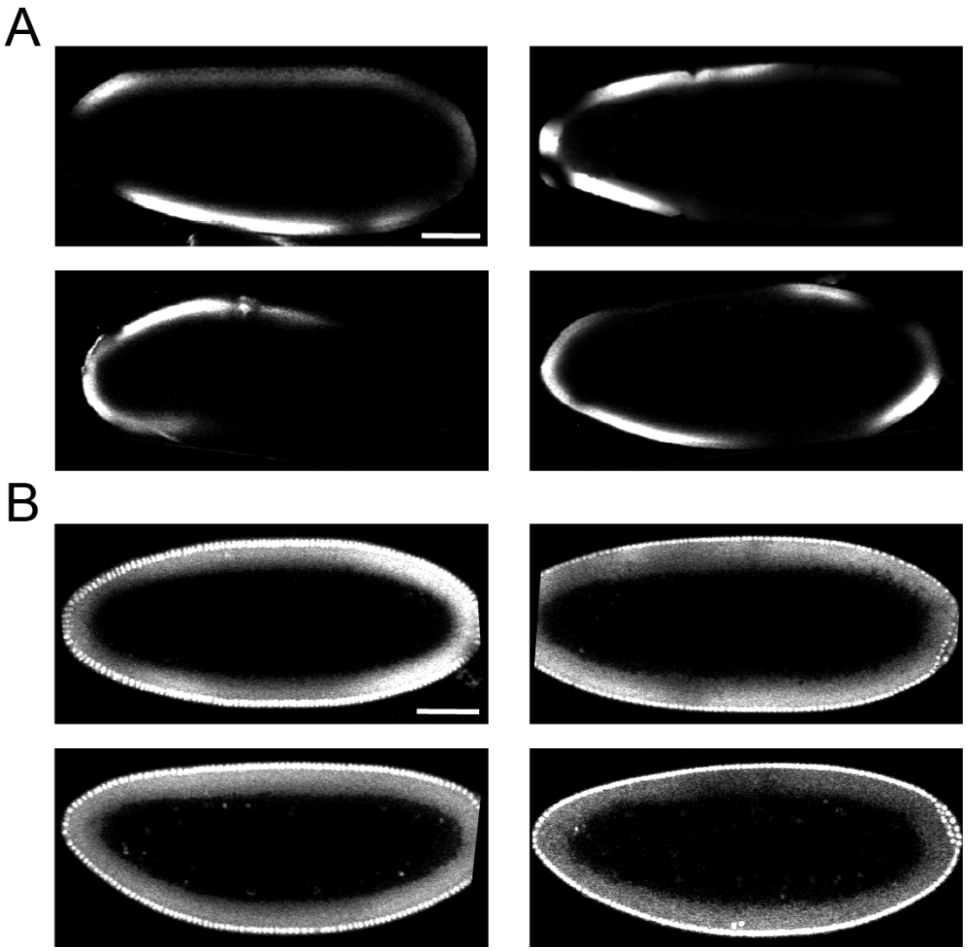

Fig.S9 Comparison of the staining efficiency of embryos with different orientations as the height of base layers is 0.045 mm (A) or 0.09 mm (B). Scale bar, 50 μm. All embryos were laid with the anterior pole on the left and the posterior pole on the right.

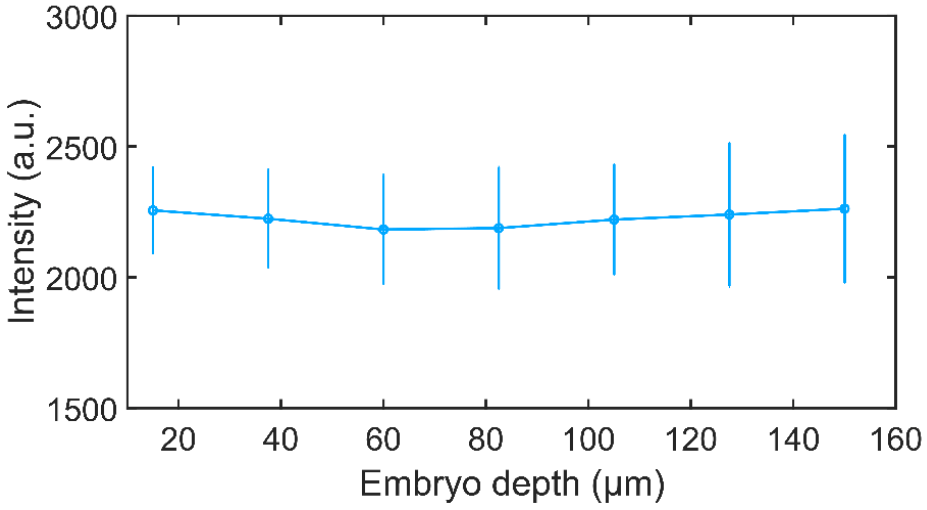

Fig. S10 The average nuclear DAPI intensity as the function of the embryo depth after depth correction with previous method,[1] i.e., use the off-chip stained embryo as a control to measure the decay of the nuclear DAPI intensity as a function of the imaging depth, normalize the intensity at different depth by the maximum intensity at the top surface, obtain the depth correction factor, which is the reciprocal of the relative intensity at the corresponding depth, and multiply the depth correction factor with the signal intensity of the on-chip stained embryo at corresponding depth. Error bars represent the standard deviation (N=4).

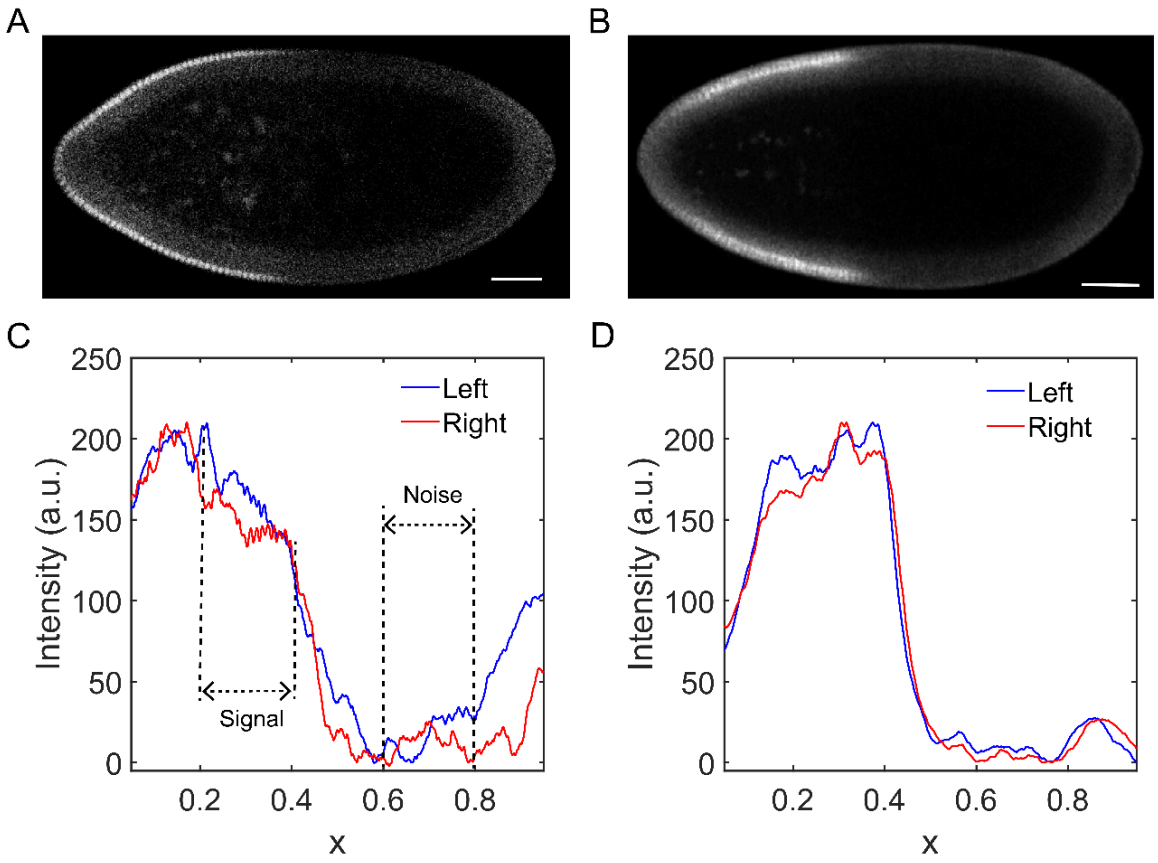

Fig. S11 On-chip and off-chip methods are comparable in IF staining efficiency. (A-B) The raw images of Hb in the WT embryos with (A) the traditional off-chip or (B) on-chip IF methods. Scale bar, 50 μm. To run the SNR analysis of the image, the signal and noise are extracted from the mean nuclear fluorescence intensity in the region with the high gene expression (e.g., $0.2< x < 0.4$ for Hb) and no expression (e.g., $0.6< x < 0.8$ for Hb), respectively. (C-D) The normalized Hb intensity profiles of the embryos with (C) the traditional off-chip or (D) on-chip IF methods.

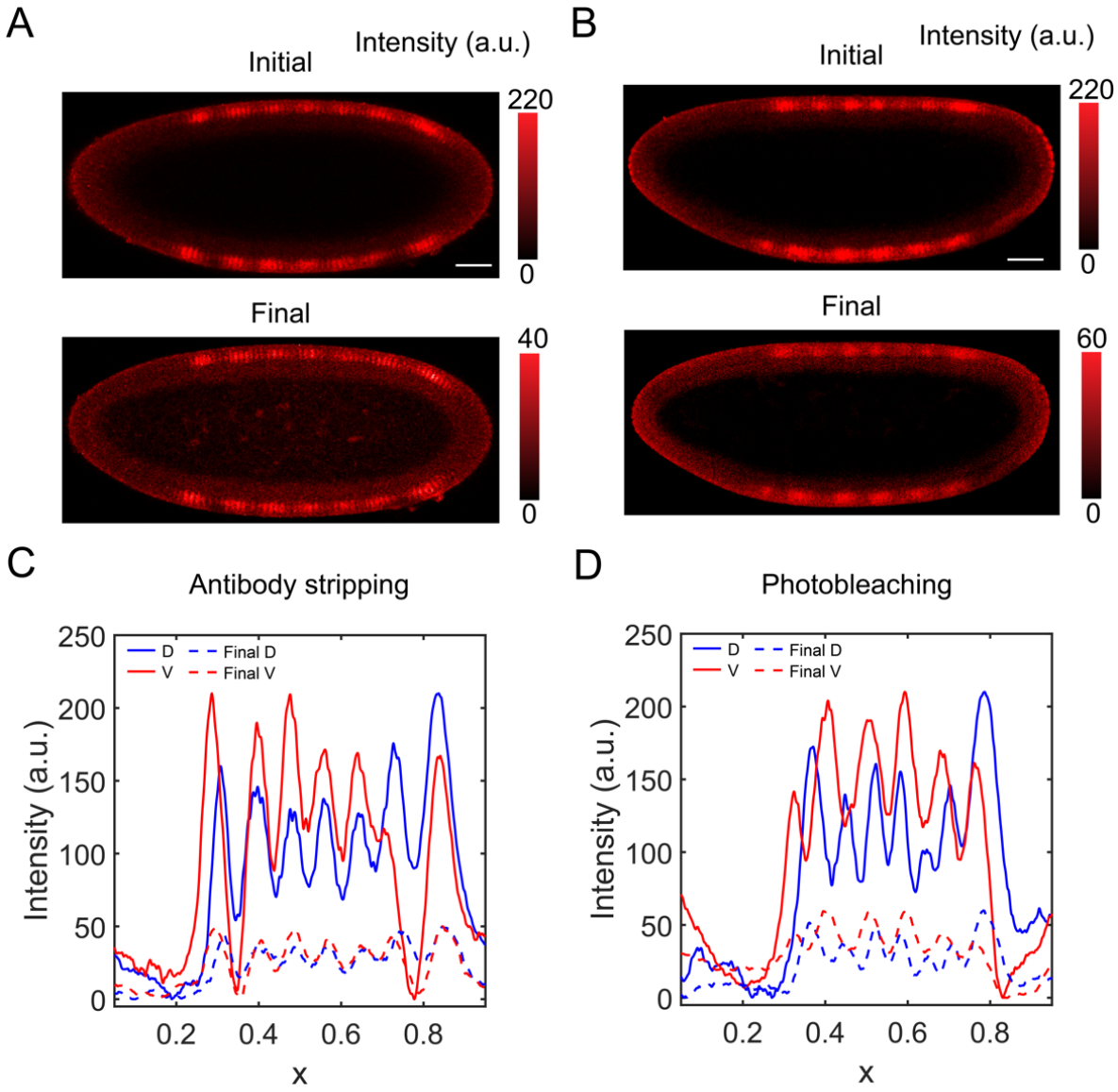

Fig. S12 Comparison of different antibody de-staining methods. (A-B) The raw images of Eve before (top) and after (bottom) antibody stripping. The color bar denotes the respective dynamic range of the intensity. Scale bar, 50 μm. (C-D) The gene expression profiles extracted from the images shown in (A-B).

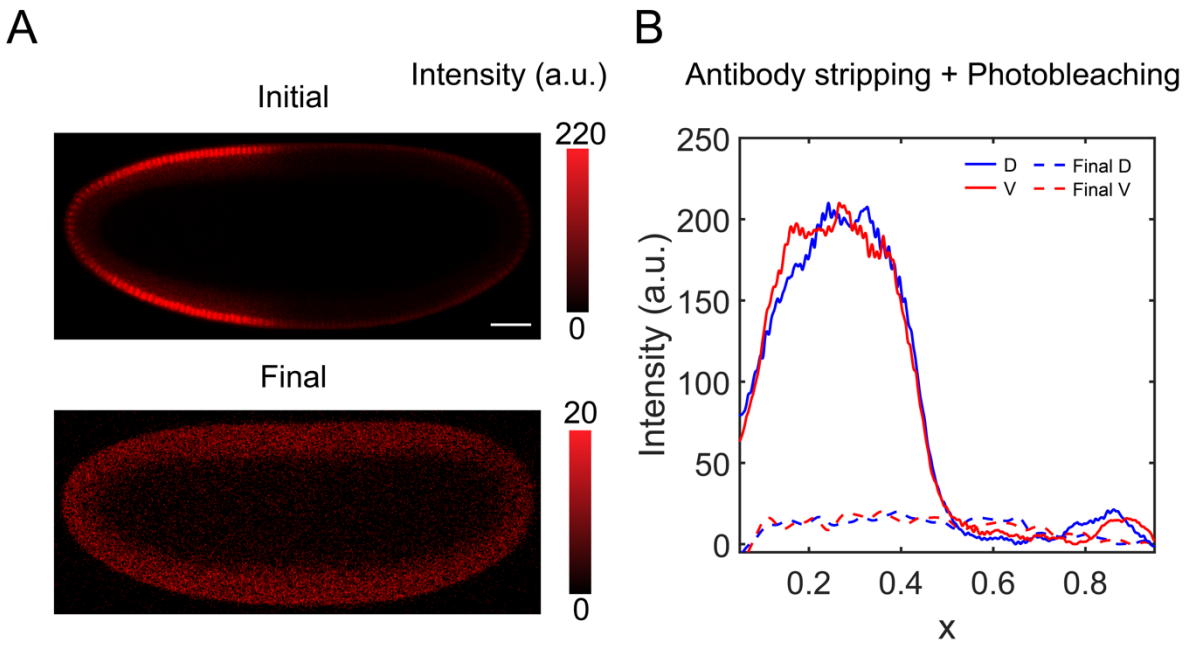

Fig. S13 Antibody de-staining effect for Hb staining embryos. (A) The raw images of a fixed WT fly embryo with IF staining on Hb before (top) and after (bottom) antibody stripping followed by photobleaching. Scale bar, 50 μm. (B) The gene expression profiles extracted from the images shown in (A).

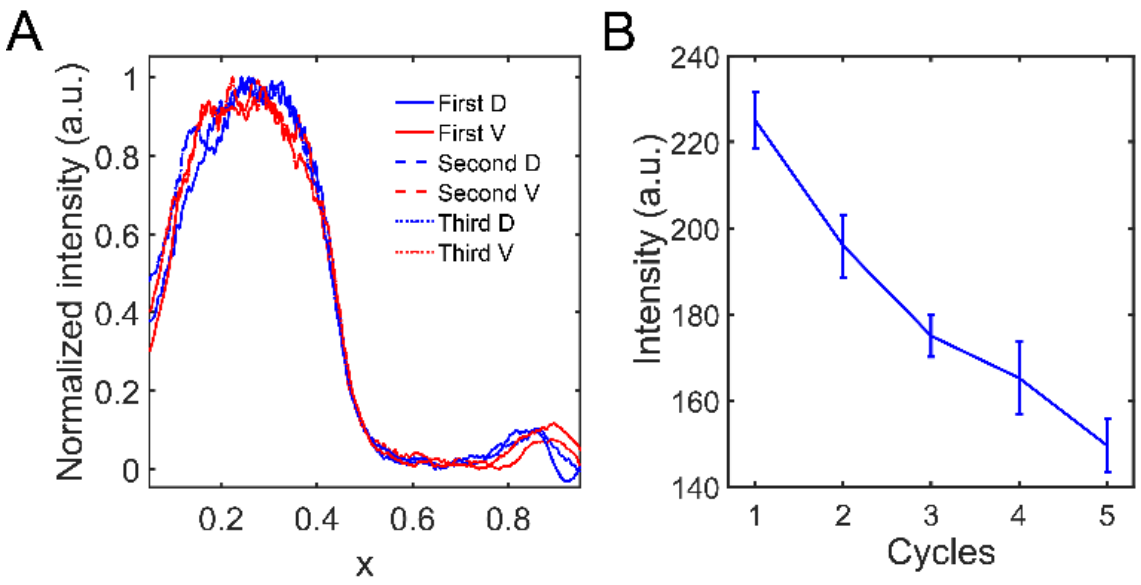

Fig. S14 Fluorescence profiles and intensity measurements via multiple cycles of immunostaining and de-staining processes. (A) The normalized Hb intensity profiles of the same embryo with three cycles of immunostaining and de-staining processes. (B) The average fluorescence intensity of the Hb ($0.2< x < 0.4$) and Eve (peak intensity of strips) as a function of five cycles of IF staining and de-staining processes. Error bars represent the standard deviation (N=5).

Movie S1 Normal development of live embryos expressing Bcd-GFP trapped in the microfluidic device observed with a confocal microscope at the excitation wavelength of 488 nm.

Movie S2 3D reconstruction of the IF images of DAPI of a WT embryo at early nuclear cycle (n.c.) 14 in the microfluidic device observed with a two-photon microscope at the excitation wavelength of 800 nm (the interval of the *z*-stack: 1 μm).

Movie S3 3D reconstruction of the IF images of DAPI of a WT embryo at mid n.c. 14 in the microfluidic device observed with a two-photon microscope at the excitation wavelength of 800 nm.

Movie S4 3D reconstruction of the IF images of DAPI of a WT embryo at late n.c. 14 in the microfluidic device observed with a two-photon microscope at the excitation wavelength of 800 nm.

Movie S5 3D reconstruction of the IF images of DAPI of a WT embryo with microfluidic device staining observed with a light-sheet microscope from two opposite directions with previous method.[1]

Movie S6 The *z*-stack (interval: 1 μm) of the IF images of Hb of a WT embryo in the microfluidic device observed with a confocal microscope at the excitation wavelength of 488 nm.

Movie S7 The *z*-stack (interval: 1 μm) of the IF images of Eve of a WT embryo in the microfluidic device observed with a confocal microscope at the excitation wavelength of 638 nm.

Table S1. Comparison of protein de-staining methods in *Drosophila* embryos.

Category	Experimental condition	Effect (Fluorescence intensity decrease ratio *R**)
Antibody removal	pH 2.8 IgG elution buffer (Thermo Scientific) and 0.5% SDS (Sigma Aldrich) [2]	79.6 ± 3.5 %
	0.94 g glycine in 25 ml 20% SDS in 500 ml distilled water (pH 2 with HCl)[3]	74.3 ± 2.4 %
	0.2% Papain and 0.2% Pepsin[4]	70.8 ± 3.5 %
	0.15 M KMnO4/0.01 M H2SO4 solution[5, 6]	Cannot image due to the dark solution color
Fluorophore bleach	Bleach the fluorophore by corresponding wavelength excitation with high power[7] (before adding the secondary antibody)	95.7 ± 4.8 %
	Bleach the fluorophore by corresponding wavelength excitation with high power[7] (after adding the secondary antibody)	78.3 ± 5 %
	3% H_2O_2 and HCl in PBS (pH 2.5)[4]	71.9± 4 %

$*R = \left(1 - \frac{Intensity\ after\ processing}{Inital\ intensity}\right) \times 100\%.$

Table S2. The embryo trapping data. 1~5 embryos were loaded at one time.

Loaded embryo number	Trapped embryo number	Trapping rate (%)
16	14	87.50
17	15	88.24
16	15	93.75
17	14	82.35
17	15	88.24
17	15	88.24
15	14	93.33
17	15	88.24
16	14	87.50
16	15	93.75
15	15	100.00
16	15	93.75
15	15	100.00
16.15*	14.69	91.14

*The last row is the average value of all rows above, respectively.

Reference

1. Z. Yang, H. C. Zhu, K. Kong, X. X. Wu, J. Y. Chen, P. Y. Li, J. L. Jiang, J. C. Zhao, B. F. Cui and F. Liu, *Elife*, 2020, **9**, e54276.
2. P. Zrazhevskiy and X. Gao, *Nat Commun*, 2013, **4**, 1619.
3. D. Pirici, L. Mogoanta, S. Kumar-Singh, I. Pirici, C. Margaritescu, C. Simionescu and R. Stanescu, *J. Histochem. Cytochem.*, 2009, **57**, 567-575.
4. J. R. Lin, M. Fallahi-Sichani and P. K. Sorger, *Nat Commun*, 2015, **6**, 8390.
5. G. Glass, J. A. Papin and J. W. Mandell, *J. Histochem. Cytochem.*, 2009, **57**, 899-905.
6. T. Tsujikawa, S. Kumar, R. N. Borkar, V. Azimi, G. Thibault, Y. H. Chang, A. Balter, R. Kawashima, G. Choe, D. Sauer, E. El Rassi, D. R. Clayburgh, M. F. Kulesz-Martin, E. R. Lutz, L. Zheng, E. M. Jaffee, P. Leyshock, A. A. Margolin, M. Mori, J. W. Gray, P. W. Flint and L. M. Coussens, *Cell Rep.*, 2017, **19**, 203-217.
7. W. Schubert, B. Bonnekoh, A. J. Pommer, L. Philipsen, R. Bockelmann, Y. Malykh, H. Gollnick, M. Friedenberger, M. Bode and A. W. Dress, *Nat. Biotechnol.*, 2006, **24**, 1270-1278.